

Four-component relativistic density functional theory with the polarisable continuum model: application to EPR parameters and paramagnetic NMR shifts

Roberto Di Remigio^a, Michal Repisky^a, Stanislav Komorovsky^a, Peter Hrobarik^b, Luca Frediani^a and Kenneth Ruud^a

^aDepartment of Chemistry, Centre for Theoretical and Computational Chemistry, University of Tromsø– The Arctic University of Norway, Tromsø, Norway; ^bInstitut für Chemie, Technische Universität Berlin, Berlin, Germany

ABSTRACT

The description of chemical phenomena in solution is as challenging as it is important for the accurate calculation of molecular properties. Here, we present the implementation of the polarisable continuum model (PCM) in the four-component Dirac–Kohn–Sham density functional theory framework, offering a cost-effective way to concurrently model solvent and relativistic effects. The implementation is based on the matrix representation of the Dirac–Coulomb Hamiltonian in the basis of restricted kinetically balanced Gaussian-type functions, exploiting a non-collinear Kramer’s unrestricted formalism implemented in the program *ReSpect*, and the integral equation formalism of the PCM available through the stand-alone library *PCMSolver*. Calculations of electron paramagnetic resonance parameters (*g*-tensors and hyperfine coupling *A*-tensors), as well as of the temperature-dependent contribution to paramagnetic nuclear magnetic resonance (pNMR) shifts, are presented to validate the model and to demonstrate the importance of taking both relativistic and solvent effects into account for magnetic properties. As shown for selected Ru and Os complexes, the solvent shifts may amount to as much as 25% of the gas-phase values for *g*-tensor components and even more for pNMR shifts in some extreme cases.

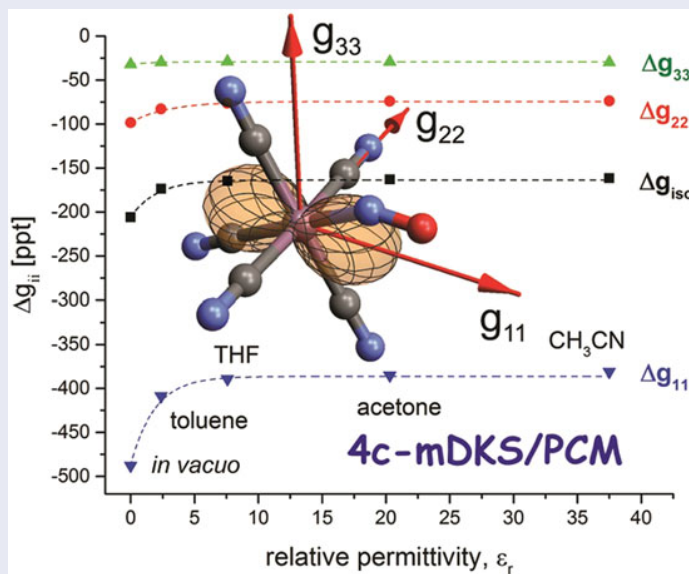
ARTICLE HISTORY

Received 30 June 2016

Accepted 16 September 2016

KEYWORDS

Relativity;
Dirac–Kohn–Sham; EPR;
paramagnetic; NMR





1. Introduction

Electron paramagnetic resonance (EPR) spectroscopy [1] is a powerful technique to unravel the structure and spin density of molecules with unpaired electrons [2,3]. Chemical reactivity is often associated with radical

intermediates, and EPR can be used to identify short-lived species in catalytic processes, also in rather complex biological or bioinorganic systems [4]. The analysis of experimental EPR spectra may be difficult, and this process can be substantially facilitated by comparing observed spectra with computed EPR parameters

CONTACT Michal Repisky ✉ michal.repisky@uit.no; Kenneth Ruud ✉ kenneth.ruud@uit.no

 Supplemental data for this article can be accessed at  http://dx.doi.org/10.1080/00268976.2016.1239846.

© 2016 Informa UK Limited, trading as Taylor & Francis Group

(see e.g. [5]). The EPR parameters most commonly studied using computational methods are the hyperfine coupling (HFC) tensors and the electronic g -tensor, which measure the coupling between the effective electron spin of the system and the nuclear magnetic moments or an external magnetic field, respectively [1]. However, other interaction mechanisms can also be observed in the experimental EPR spectra, such as the zero-field splitting (ZFS) due to the interaction between two electron spins in the case of triplet or higher spin multiplicities [1].

Although the EPR parameters are inherently relativistic in nature, their calculation by means of perturbation theory performs well for molecules with light elements. Studies have been presented both at the level of density functional theory (DFT), either in a spin-unrestricted [6–11] or a spin-restricted approach [12–14], and at the level of multi-configurational methods [15–21]. However, for systems with very large relativistic corrections, of which the most important for EPR spectroscopy is the spin–orbit (SO) coupling, the perturbation-based methods fail to reproduce not only the magnitude but also the sign of certain EPR tensor components due to the large sensitivity of these parameters on higher -order SO effects [22–24]. Moreover, the SO coupling may be so strong that there is no longer a direct connection between the spin density and the observed or calculated EPR parameters, mandating an accurate and realistic computational protocol to interpret EPR measurements correctly. Among the efficient electronic structure methods capable of predicting EPR parameters for larger systems, such as transition metal complexes, DFT has already proved its usefulness, in particular when combined with relativistic quantum mechanics based on approximate quasi-relativistic (two-component) Hamiltonians or even the full (four-component) Dirac Hamiltonian. By this, higher -order SO relativistic corrections are included from the start in the variational framework. Several two-component DFT implementations have been reported, involving either the zeroth-order regular approximation (ZORA) or the Douglas–Kroll–Hess (DKH) Hamiltonians. In such studies, spin polarisation effects, which are highly relevant for EPR calculations, were either excluded (Kramer’s restricted approach) [25–27] or included (Kramer’s unrestricted approach) [28–32]. More recently, four-component calculations of EPR parameters became available [24,33–37], with their clear advantage over two-component methods not only in higher precision but also in the absence of complicated picture-change transformations of magnetic operators [28–30].

The calculation of paramagnetic nuclear magnetic resonance (pNMR) parameters can be directly related to

the parameters of an EPR spin Hamiltonian, as shown for doublet systems by Moon and Patchkovskii [38] and later extended to systems with an arbitrary degeneracy by Van Den Heuvel and Soncini [39]. The recourse to EPR parameters is, however, not necessary as revealed in a comprehensive pNMR theory by Van Den Heuvel and Soncini [40] and supported by applications to heavy-metal-containing systems by Gendron *et al.* [41]. Over time, relativistic effects have been included in the calculation of pNMR parameters of increasing quality: from perturbation corrections [42,43], via the ZORA Hamiltonian [44] up to the four-component Dirac–Coulomb Hamiltonian [45]. Despite these successes, ZFS effects have only recently been included in the calculation of pNMR shifts for systems with multiplicities higher than a doublet [41,46,47], following the theory derived from first principles [40].

The majority of chemical experiments, including EPR and pNMR spectroscopic measurements, happen in solution or in complex environments [48]. This is challenging for quantum–chemical calculations: to reproduce experimental observations, solvent effects must be included, especially for molecular properties that are sensitive to the environment, such as (p)NMR and EPR parameters [49–52]. However, a full quantum treatment of the solvent is not possible, both because of the large number of solvent molecules that must be included in the solvent model, and because of the dynamics of the solvent systems. The conceptually simplest approach is to include (parts of) the environment explicitly [53]. Such *cluster methods* include all relevant intermolecular interactions at the same quantum–chemical level of theory, but it is difficult to achieve convergence with respect to the size of the cluster. Moreover, sampling of the huge conformational space will be computationally expensive and in many cases difficult to achieve.

Focused models offer a practical alternative to include environment effects in quantum–chemical calculations: only a small part of the full system is treated quantum mechanically, whereas the rest is modelled in an approximate way, retaining only the environment effect on the electronic structure of the relevant solvated system. Two main approaches can be identified: quantum mechanics/molecular mechanics (QM/MM) methods [54] and dielectric continuum (DC) methods [55].

In QM/MM methods, both solute and solvent are represented with atomistic details. However, the solute is treated quantum mechanically whereas the solvent molecules are treated with a classical force field [54]. Although the QM/MM methods have received considerable popularity and several works have recently been devoted to QM/MM modelling of electronic g -tensors and HFC constants of paramagnetic species in solution

[56–61], various questions related to the number of snapshots required to reach convergence of different properties or the size of the solvation shell remain difficult to answer. These aspects have limited the use of the QM/MM methodology as a widespread black-box computational protocol.

In DC models, the solvent molecules are replaced by a structureless continuum characterised by its bulk properties [55,62]. Continuum models, and the polarisable continuum model (PCM) foremost among these, include only electrostatic solute–solvent interactions in their basic formulations, though other effects can be included [63,64]. In contrast to the cluster and QM/MM methods, long-range electrostatics and statistical averaging are already included in the continuum formulation. Several applications, combining magnetic properties and the continuum models for the inclusion of solvent effects, have been presented at the non-relativistic or relativistic perturbational level of theory (see e.g. [56,65,66], review papers [50–52] and references therein), mostly for organic free radicals because of their ubiquity in biological systems and their relevance as spin probes.

EPR and pNMR spectroscopies are also valuable for compounds containing heavy elements. The importance of relativistic and solvent effects on magnetic resonance parameters is recognised both experimentally and computationally [51,67–75]. Heavy-element-containing compounds are often large, and in order to treat these compounds in solution, the computational protocol must be cost efficient and able to reliably describe both the effects of the environment and relativity. Several groups extensively studied strategies for the calculation of NMR shieldings and nuclear spin–spin couplings using the ZORA or Dirac–Coulomb Hamiltonians. They have used both cluster [68] and cluster/continuum [69,74,75] models to describe solvent effects, as well as Born–Oppenheimer molecular dynamics [71,73] to include additional dynamical effects. All these studies point towards the importance of including at least bulk solvent effects in the computational protocol to achieve agreement with experimentally observed trends.

The main goal of the present work is to bridge the existing gap in computational methodologies and to offer a cost-effective way to concurrently model direct solvent effects and relativistic effects in EPR and pNMR calculations of paramagnetic species. To accomplish this, we extended a recent implementation of the PCM self-consistent field (SCF) scheme at the relativistic four-component DFT level of theory [76] to the Kramer’s unrestricted regime and assessed the methodology in calculations of EPR *g*- and *A*-tensors, as well as the temperature-dependent contribution to pNMR shifts. The implementation is done in the ReSpecT [77] program package

and utilises the same modular strategy as exploited in the DIRAC implementation [76]: the PCM functionality is provided by an interface to the independently developed PCMSolver library [78].

The rest of the paper is organised as follows. In Section 2, we present the theoretical foundation for our implementation of the PCM in the calculation of EPR and pNMR parameters at the four-component level of theory. In Section 3, we summarise the computational details, before we present in Section 4, the results of pilot applications. Finally, in Section 5, we give some concluding remarks and an outlook. Note that atomic units will be used throughout the text.

2. Theory

2.1. IEF-PCM

Continuum solvation models are among the simplest focused models for the description of solvent effects [55,62,79]. The solvent is replaced by a structureless continuum, described by macroscopic physical properties. The solute is placed in a cavity inside the continuum and the mutual electrostatic polarisation of the solute and the solvent is taken into account by means of a continuous electric field, called the *reaction field*, that is modulated by the bulk permittivity of the solvent.

This is a problem of classical electrostatics: given a closed volume V with boundary ∂V inside a dielectric of permittivity ϵ_r and fully enclosing a charge density ρ_0 , find the corresponding electrostatic potential $\psi(\mathbf{r})$ in space [80,81]:

$$\begin{cases} \nabla^2 \psi(\mathbf{r}) = -4\pi \rho_0(\mathbf{r}) & \forall \mathbf{r} \in V \\ \epsilon_r \nabla^2 \psi(\mathbf{r}) = 0 & \forall \mathbf{r} \notin V \\ \lim_{|\mathbf{r}| \rightarrow \partial V^+} \psi(\mathbf{r}) = \lim_{|\mathbf{r}| \rightarrow \partial V^-} \psi(\mathbf{r}) \\ \epsilon_r \lim_{|\mathbf{r}| \rightarrow \partial V^+} \frac{\partial \psi(\mathbf{r})}{\partial \hat{\mathbf{n}}} = \lim_{|\mathbf{r}| \rightarrow \partial V^-} \frac{\partial \psi(\mathbf{r})}{\partial \hat{\mathbf{n}}} \end{cases} \quad (1)$$

The first and second partial differential equations (PDEs) are augmented by the last two equations that impose the proper boundary conditions. We require that $\psi(\mathbf{r})$ is continuous across the cavity boundary and that its directional derivative has a finite jump, related to the permittivity constant ϵ_r , across the cavity boundary. The directional derivatives are taken with respect to the surface normal vector $\hat{\mathbf{n}}$, from the inside (subscript +) and from the outside (subscript –) relative to the cavity boundary.

In the integral equation formalism (IEF) of the PCM [82], the system in Equation (1) is recast as an integral equation [83,84] whose domain is the surface of the

cavity boundary ∂V , a 2-manifold. We represent the electrostatic potential as

$$\psi(\mathbf{r}) = \int_V d^3\mathbf{r}' \frac{\rho_0(\mathbf{r}')}{|\mathbf{r} - \mathbf{r}'|} + \int_{\partial V} d\mathbf{t} \frac{\sigma(\mathbf{t})}{|\mathbf{r} - \mathbf{t}|} = \varphi + \xi, \quad (2)$$

where φ is the Newton potential, i. e. the molecular electrostatic potential (MEP) generated by ρ_0 *in vacuo*. The second term is the *reaction field* and is parametrised in terms of the apparent surface charge (ASC) $\sigma(\mathbf{t})$, a charge distribution spread over the cavity boundary. It can be shown that the ASC is the unique solution to the integral equation [82]

$$\left[2\pi \left(\frac{\varepsilon_r + 1}{\varepsilon_r - 1} \right) \hat{\mathcal{I}} - \hat{\mathcal{D}} \right] \hat{\mathcal{S}}\sigma = - \left(2\pi \hat{\mathcal{I}} - \hat{\mathcal{D}} \right) \varphi, \quad (3)$$

where the integral operators are expressed by means of the Green's function for the differential operator in Equation (1):

$$\begin{aligned} (\hat{\mathcal{S}}f)(\mathbf{t}) &= \int_{\partial V} d\mathbf{t}' G(\mathbf{t}, \mathbf{t}') f(\mathbf{t}'), \\ (\hat{\mathcal{D}}f)(\mathbf{t}) &= \int_{\partial V} d\mathbf{t}' [\nabla_{\mathbf{t}'} G(\mathbf{t}, \mathbf{t}') f(\mathbf{t}')] \cdot \hat{\mathbf{n}}_{\mathbf{t}'}, \\ G(\mathbf{r}, \mathbf{r}') &= \frac{1}{|\mathbf{r} - \mathbf{r}'|} \end{aligned} \quad (4)$$

with $\hat{\mathcal{I}}$ being the identity operator. The ASC fully determines the reaction field and the mutual polarisation between the solute and the solvent. Furthermore, the full three-dimensional problem in Equation (1) has been reduced to the determination of a scalar function of the surface coordinate \mathbf{t} . The integral equation formalism is also quite general: knowledge of the boundary conditions and the Green's function for any linear, elliptic PDE is sufficient in order to set up the associated integral equation. IEF-PCM is not restricted to homogeneous, uniform dielectrics, and extensions have been presented for ionic liquids and liquid crystals [82], dielectric interfaces [85,86] and metal nanoparticles [87].

The boundary element method (BEM) is the standard method to solve integral equations such as the IEF-PCM equation (3). The surface of the molecular cavity is discretised into finite elements with a basis set of piecewise regular functions attached [88]. It is then possible to discretise the integral operators $\hat{\mathcal{S}}$ and $\hat{\mathcal{D}}$, the unknown ASC σ and the MEP φ . This leads to a linear system of equations [83]. In our implementation [78], we use the GePol algorithm to discretise the cavity boundary. In this approach [89], the cavity is defined as a set of interlocking spheres which are divided into N_{ts} spherical triangles Δ_i by means of an equilateral partitioning

algorithm. We apply a parametrised, one-point, collocation scheme [55,90] to obtain the linear system of equations. The centroids of the spherical triangles are chosen as collocation points. Eventually, the linear equations are solved by direct LU decomposition. Detailed expressions for the matrix elements of the discretised boundary integral operators can be found in [55,90].

We note at this point that the conductor-like screening model (COSMO) [91–93] is a special case of Equation (3), and the COSMO equation [93]

$$\hat{\mathcal{S}}\sigma = -f(\varepsilon_r)\varphi, \quad (5)$$

can be obtained by taking the infinite-permittivity limit of Equation (3), or starting from Equation (1) and assuming conductor-like boundary conditions. The correction factor $f(\varepsilon_r) = \frac{\varepsilon_r - 1}{\varepsilon_r + X}$ ($0 \leq X \leq 1$) is added to account for the fact that the solvent is a dielectric medium rather than a proper conductor.

2.2. Four-component EPR theory

The theoretical foundations for the calculation of the EPR \mathbf{g} -tensor and HFC \mathbf{A} -tensor in the framework of four-component Dirac–Kohn–Sham (DKS) theory have been described previously [35,36]. Here we will only briefly recapitulate the details of the implementation in the ResPECT program package [77]. In the following, we will assume summation over repeated indices and adopt the following notation: the indices λ, τ, μ, ν will denote atomic orbitals (AO), u, v will denote Cartesian components of tensors and i will be used as index for occupied molecular orbitals (MO).

The EPR \mathbf{g} - and \mathbf{A} -tensors are calculated in four-component theory as first-order molecular properties, which is equivalent for variational methods such as DKS to the calculation of an expectation value by virtue of the Hellmann–Feynman theorem [94]

$$g_{uv} = \frac{2c}{\langle \tilde{S}_v \rangle} \text{Tr} \{ \mathbf{\Lambda}_{B_u} \mathbf{D}^{(J_v)} \}, \quad (6)$$

$$A_{uv}^M = \frac{1}{\langle \tilde{S}_v \rangle} \text{Tr} \{ \mathbf{\Lambda}_{I_u^M} \mathbf{D}^{(J_v)} \}. \quad (7)$$

Here, c is the speed of light and $\langle \tilde{S}_v \rangle$ is an effective spin of the system. The matrices with elements $\mathbf{\Lambda}_{\lambda\tau}$ are the four-component representation of the perturbation operators in a restricted kinetically balanced (RKB) basis set:

$$(\mathbf{\Lambda}_{B_u})_{\lambda\tau} = \frac{1}{2} \langle \mathbf{X}_\lambda | (\mathbf{r}_G \times \boldsymbol{\alpha})_u | \mathbf{X}_\tau \rangle, \quad (8)$$

$$\left(\Lambda_{I_u^M}^{\text{PN}}\right)_{\lambda\tau} = \gamma^M \left\langle X_\lambda \left| \left(\frac{\mathbf{r}_M \times \boldsymbol{\alpha}}{r_M^3} \right)_u \right| X_\tau \right\rangle, \quad (9)$$

$$\left(\Lambda_{I_u^M}^{\text{FN}}\right)_{\lambda\tau} = \gamma^M \left\langle X_\lambda \left| \left[\boldsymbol{\alpha} \times \nabla \int \left(\frac{\eta}{\pi} \right)^{3/2} \frac{e^{-\eta(\mathbf{R}-\mathbf{R}_M)^2}}{|\mathbf{r}-\mathbf{R}|} d^3\mathbf{R} \right]_u \right| X_\tau \right\rangle, \quad (10)$$

\mathbf{r}_M (\mathbf{r}_G) is the electron position vector \mathbf{r} relative to the coordinates of the M th nucleus \mathbf{R}_M (gauge origin \mathbf{R}_G). The Dirac matrices $\boldsymbol{\alpha}$ and $\boldsymbol{\beta}$ are composed of the two-by-two zero (0_2), unit (1_2) and Pauli spin matrices $\boldsymbol{\sigma} = (\sigma_x, \sigma_y, \sigma_z)$:

$$\boldsymbol{\alpha} = \begin{pmatrix} 0_2 & \boldsymbol{\sigma} \\ \boldsymbol{\sigma} & 0_2 \end{pmatrix}, \quad \boldsymbol{\beta} = \begin{pmatrix} 1_2 & 0_2 \\ 0_2 & -1_2 \end{pmatrix}. \quad (11)$$

Although we provide expressions for both point nucleus (PN) (Equation (9)) and finite nucleus (FN) (Equation (10)) models of the magnetic moment distribution, in the present work, only the PN model was used. The effects of these two models in the four-component calculations of the \mathbf{A} -tensor have been discussed in [36]. The RKB basis has the four-by-four matrix form

$$X_\lambda = \begin{pmatrix} 1_2 & 0_2 \\ 0_2 & \frac{1}{2c} \boldsymbol{\sigma} \cdot \mathbf{p} \end{pmatrix} \chi_\lambda, \quad (12)$$

with χ_λ representing a Gaussian-type scalar function, $\boldsymbol{\sigma}$ is the vector composed of Pauli matrices and \mathbf{p} is the momentum operator.

The one-particle density matrix in Equations (6) and (7) is defined as

$$D_{\lambda\tau}^{(J_b)} = C_{\lambda i}^{(J_b)} C_{\tau i}^{(J_b)\dagger}, \quad (13)$$

where the occupied molecular orbital coefficients $C_{\lambda i}$ are obtained from the four-component analogue of the Roothaan–Hall equations

$$\mathbf{F}^{(J_b)} \mathbf{C}^{(J_b)} = \mathbf{S} \mathbf{C}^{(J_b)} \boldsymbol{\epsilon}^{(J_b)}, \quad (14)$$

where \mathbf{S} is the overlap matrix, defined as

$$S_{\lambda\tau} = \langle X_\lambda | X_\tau \rangle, \quad (15)$$

and $\boldsymbol{\epsilon}^{(J_b)}$ the orbital (one-electron) energies [95,96].

The superscript (J_b) indicates the dependence of the molecular orbitals on the orientation of the magnetisation vector \mathbf{J} . If the magnetisation vector is oriented along the principal axes of the \mathbf{g} -tensor, the calculation of the \mathbf{g} - and \mathbf{A} -tensors will only require three solutions of the Kramer's unrestricted Roothaan–Hall equation (14). From each solution, one diagonal component of the \mathbf{g} -tensor and one column of the \mathbf{A} -tensor are obtained. However, this approach requires that the principal axes of the \mathbf{g} -tensor are known prior to the calculations. In case of systems with high symmetry, such as the $[\text{ReNX}_n]^-$ complexes studied in this work, the orientation of the \mathbf{g} -tensor principal axes is known *a priori* and coincides with symmetry axes. In more general cases, results from preliminary one-component perturbation calculations can be used as starting guess. Subsequently, a series of four-component calculations are carried out and after each calculation, the \mathbf{g} -tensor is rotated and new principal axes are determined. The orientation of the principal axes is usually converged in a single iteration. A more detailed discussion of four-component \mathbf{g} -tensor calculations and the differences between Kramer's restricted and unrestricted methods can be found in [35,97].

In the following, we will omit the (J_b) superscript to simplify the notation. The Dirac–Hartree–Fock (DHF, $\theta = 1$) or Dirac–Kohn–Sham ($0 \leq \theta < 1$) vacuum Fock matrix can be divided into one- and two-electron contributions:

$$F_{\text{vac}} = h^D + G[\theta, D] + V^{\text{xc}}[(1 - \theta), D]. \quad (16)$$

h^D represents the one-electron Dirac Hamiltonian in the RKB basis

$$h_{\lambda\tau}^D = \langle X_\lambda | c\boldsymbol{\alpha} \cdot \mathbf{p} + (\beta - 1_4)c^2 + V^{\text{nuc}} 1_4 | X_\tau \rangle, \quad (17)$$

with $\boldsymbol{\alpha}$ and $\boldsymbol{\beta}$ matrices defined by Equation (11), and the scalar nuclear–electron attraction potential operator

$$V^{\text{nuc}} = - \sum_M Z_M \int \left(\frac{\eta}{\pi} \right)^{3/2} \frac{e^{-\eta(\mathbf{R}-\mathbf{R}_M)^2}}{|\mathbf{r}-\mathbf{R}|} d^3\mathbf{R}, \quad (18)$$

and Z_M the nuclear charge. Here, we have assumed a finite-sized nuclear model of Gaussian type where both the nuclear charge and magnetic moment distributions are modelled with the same s -type Gaussian function. This approximation is justified because the \mathbf{A} -tensor is only weakly dependent on the particular finite magnetic moment distribution [98]. The two-electron contribution \mathbf{G} describes the instantaneous Coulomb electron–electron interaction. It consists of a Coulomb (\mathbf{J}) and an exchange part (\mathbf{K})

$$G[\theta] = J - \theta K, \quad (19)$$

$$J_{\lambda\tau} = \iint \frac{\Omega_{\lambda\tau}(\mathbf{r}) D_{\mu\nu} \Omega_{\nu\mu}(\mathbf{r}')}{|\mathbf{r} - \mathbf{r}'|} d^3\mathbf{r} d^3\mathbf{r}', \quad (20)$$

$$K_{\lambda\tau} = \iint \frac{\Omega_{\lambda\mu}(\mathbf{r}) D_{\mu\nu} \Omega_{\nu\tau}(\mathbf{r}')}{|\mathbf{r} - \mathbf{r}'|} d^3\mathbf{r} d^3\mathbf{r}', \quad (21)$$

where \mathbf{r} and \mathbf{r}' are variables in \mathbb{R}^3 , and $\Omega_{\lambda\tau} = \mathbf{X}_\lambda^\dagger \mathbf{X}_\tau$ is the overlap distribution of two four-component basis functions, as defined in Equation (12). Note that the order of the four-by-four matrices in the numerator of Equation (21) is fixed, since they do not commute.

The construction of the Fock matrix equation (16) requires the non-collinear exchange–correlation (XC) potential for generalised gradient approximation (GGA) functionals. In our implementation, we use the following definition of the non-collinear XC potential

$$V_{\lambda\tau}^{\text{xc}} = \int \left(\frac{\partial \epsilon^{\text{xc}}}{\partial n} \Omega_{\lambda\tau} + \frac{\partial \epsilon^{\text{xc}}}{\partial s} \frac{\rho_k}{s} \Omega_{\lambda\tau}^k + \frac{\partial \epsilon^{\text{xc}}}{\partial (\nabla_i n)} \nabla_i \Omega_{\lambda\tau} + \frac{\partial \epsilon^{\text{xc}}}{\partial (\nabla_i s)} \frac{\rho_k}{s} \nabla_i \Omega_{\lambda\tau}^k \right) d^3\mathbf{r}, \quad (22)$$

where ϵ^{xc} denotes the XC energy density, which depends on the electron charge density n and the length of the electron spin density vector s

$$n = \text{Tr}[\mathbf{D}\Omega], \quad s = \sqrt{\rho_x^2 + \rho_y^2 + \rho_z^2}, \quad \rho_k = \text{Tr}[\mathbf{D}\Omega^k], \quad (23)$$

$$\Omega_{\lambda\tau}^k = \mathbf{X}_\lambda^\dagger \Sigma_k \mathbf{X}_\tau, \quad \Sigma_k = \begin{pmatrix} \sigma_k & 0_2 \\ 0_2 & \sigma_k \end{pmatrix}, \quad (24)$$

with Σ_k being the four-component spin operator. Since we consider here only systems with a degenerate ground state, both the spin density and its gradient are non-zero, in contrast to systems with a non-degenerate ground state. The form of the non-collinear XC potential for local density approximation (LDA) functionals, given by the first two terms on the right-hand side of Equation (22), has previously been presented by Sandratskii [99] and van Wüllen [100]. A straightforward extension of these LDA expressions to non-zero gradients of the spin density suffers from numerical instabilities as discussed by Scalmani and Frisch [101]. The expression in Equation (22) is both numerically stable and includes gradients of the spin density in a non-collinear fashion. The physical motivation for the definition in Equation (22), as well as a discussion of numerical instabilities, will be presented elsewhere.

The final ingredient in the construction of the Fock matrix in Equation (14) is the additional one-electron

PCM potential. Detailed derivations have already been given, both in the context of one-component [55,79] and four-component methods [76]. The vacuum Fock matrix in Equation (16) is augmented by the PCM one-electron potential

$$\mathbf{F} = \mathbf{F}_{\text{vac}} + \mathbf{V}^{\text{PCM}}, \quad (25)$$

with

$$\mathbf{V}^{\text{PCM}} = \int_{\partial V} \sigma(\mathbf{t}) \boldsymbol{\varphi}(\mathbf{t}) d\mathbf{t}. \quad (26)$$

Note that in the previous equation, σ is *not* a Pauli matrix but rather the ASC as computed by solving Equation (3). The representation of the MEP operator in a four-component RKB basis is given by

$$\boldsymbol{\varphi}_{\lambda\tau}(\mathbf{t}) = - \int \frac{\Omega_{\lambda\tau}(\mathbf{r})}{|\mathbf{r} - \mathbf{t}|} d^3\mathbf{r}. \quad (27)$$

Note that only the large–large and small–small component blocks remain non-zero because the Coulomb interaction is represented by a scalar multiplicative operator. In Equation (25), we use the non-discretised form of the PCM Fock matrix contribution, in contrast to the form presented in [76]. The two forms are equivalent, but the current formalism is more general as it does not require either a reference to the PCM model adopted (IEF-PCM or COSMO) or the use of a BEM scheme to solve the classical PCM problem.

2.3. Four-component pNMR theory

The NMR chemical shift of paramagnetic substances is in general temperature-dependent and it is, therefore, customary to decompose the total isotropic pNMR shift into two contributions

$$\delta_M = \delta_M^{\text{orb}} + \delta_M^{\text{para}}. \quad (28)$$

The orbital contribution δ_M^{orb} is approximately temperature independent (neglecting the rovibrational motion of the nuclei), in contrast to the paramagnetic contribution δ_M^{para} which usually exhibits a strong temperature dependence [102–104]. These contributions can be separated in experimental measurements by plotting the temperature dependence of the pNMR signals against $1/T$, where the slope and the intercept with the vertical axis are related to the paramagnetic and orbital contributions to the pNMR shifts, respectively. In this work, we exclusively focus on the paramagnetic contribution to the pNMR shift, which, for systems with a doubly degenerate ground state, has the

form (see [38,42])

$$\delta_M^{\text{para}} = \frac{\mu_e}{12\gamma_M kT} \text{Tr}(\mathbf{g}\mathbf{A}_M^{\text{T}}). \quad (29)$$

Here μ_e is the Bohr magneton, γ_M is the gyromagnetic ratio of nucleus M, kT is the thermal energy, and \mathbf{g} and \mathbf{A}_M are corresponding EPR tensors as defined in Equations (6) and (7). From Equation (29), it follows that accurate measurements of the paramagnetic shift provide us with an indirect link to the EPR parameters. This connection has already been examined in the framework of relativistic four-component DFT theory [45].

3. Computational details

Structures of the small Re^{VI} compounds and larger *trans*- $[\text{Ru}^{\text{III}}\text{Cl}_4(\text{DMSO})(4\text{-R-py})]^-$ complexes were taken from the Supporting Information of references [24] and [67], respectively. Structures of the Ru and Os nitrosyl complexes were optimised in the Turbomole program using the PBE0 [105,106] hybrid functional with Grimme's atom-pairwise D3 dispersion corrections [107] and Becke–Johnson (BJ) damping [108]. Quasi-relativistic energy-consistent, small-core pseudopotentials (effective-core potentials, ECP) [109] were used for the metal centres, with (7s7p5d1f)/[6s4p3d1f] and (8s7p6d1f)/[6s4p3d1f] Gaussian-type orbital valence basis sets for the 4d and 5d metal atoms, respectively. Ligand atoms were treated with an all-electron def2-TZVP basis set [110]. All the geometries are collected in the Supporting Information. The property calculations were carried out at the four-component DKS level of theory with the developers version (3.5.0) of the relativistic quantum chemistry program ReSpect [77]. The hybrid PBE0 functional and its modified form with a customised admixture of 40% Hartree–Fock exchange (PBE0-40HF) were used, respectively. In our previous studies, the PBE0-40HF functional was found to provide good agreement with experimental data, clearly outperforming GGA functionals, in particular for the HFC [24]. The exchange–correlation contribution was evaluated numerically on an integration grid consisting of 80 radial grid points and a Lebedev angular grid with an adaptive size and its rotationally invariant implementation was preserved by means of a non-collinear approach with the spin density described as the norm of the spin magnetisation vector (see Section 2.2). For all nuclei, a finite-sized Gaussian distribution model for the nuclear charge was applied with parameters taken from [111], whereas a simple point model was used for nuclear magnetic moments. To represent the large-component spinors, all-electron Gaussian-type basis sets of polarised triple-zeta quality were used: the uncontracted form of Jensen's pcJ-2 basis

for elements of the first three periods (upcJ-2) [112], and the uncontracted form of Dyall's vTZ basis set [113–115] for the heavy elements. A restricted kinetic balance condition was imposed at the integral level to construct the small-component basis. The evaluation of the two-electron contributions to the Fock matrix is the dominant computational task, especially in four-component-based methodologies. To reduce the cost of this essential step, an *atom-pair approximation* for the electron repulsion integrals was used: the evaluation of four-centre two-electron integrals over atom-centred small-component basis functions χ^{S} is discarded, unless the bra and ket basis pairs share the same origin, i.e. $[\chi_A^{\text{S}}\chi_B^{\text{S}}|\chi_C^{\text{S}}\chi_D^{\text{S}}]\delta_{AB}\delta_{CD}$, where δ is the Kronecker delta and A, B, C and D refer to the origin of the basis functions. Unless stated otherwise, the cavities used for the PCM were generated using van der Waals radii from Allinger's MM3 model [116]: 1.62 Å for H, 2.04 Å for C, 1.93 Å for N, 1.82 Å for O, 1.71 Å for F, 2.15 Å for S, 2.07 Å for Cl, 2.34 Å for Ru, 2.37 Å for Re and 2.35 Å for Os, all scaled down by a factor of 1.2. The addition of spheres not centred on the nuclei was disabled and a tessellation with an average finite element area of 0.3Å^2 was used.

4. Applications

In this study, we will only be concerned with the so-called *direct* solvent effects – that is, solvent effects arising directly from the mutual polarisation of the solvent and the solute density. *Indirect solvent effects* arising from the relaxation of the molecular structure upon solvation are not considered here. This set-up enables to ease the interpretation of the results, as they only contain direct solvent effects.

Initial validation studies of our 4c-mDKS/IEF-PCM implementation on a series of $[\text{MEX}_n]^q$ d¹ complexes, investigated previously using various relativistic approaches *in vacuo* [24], revealed a minor effect of the continuum solvent model on the EPR parameters. The results for selected Re^{VI} complexes, $[\text{ReNF}_4]^-$ and $[\text{ReNCl}_4]^-$, in the gas phase and in CH_3CN solution are presented in Table 1. The solvent shifts (the differences between EPR parameters computed with and without inclusion of the PCM solvent model) amount to only a few ppt for Δg -tensor components (with a maximum of -9 ppt for Δg_{\parallel} in $[\text{ReNF}_4]^-$) and up to 40–50 MHz for metal HFC constants. Although these solvent shifts should be considered in highly accurate EPR calculations, they are smaller or comparable to the experimental error and much less pronounced than the effect of DFT functional and/or basis set, see Table 1 and corresponding footnotes. Comparably small solvent shifts are also found for other members of the $[\text{MEX}_n]^q$ benchmark

Table 1. Effect of a polarisable continuum solvent model (IEF-PCM) on computed principal components of the electronic Δg tensor (ppt) and of the metal HFC tensor (MHz) in selected Re^{VI} complexes.^a

Complex	Method	Solvent	Δg_{\parallel}	Δg_{\perp}	Δg_{iso}	A_{\parallel}^{M}	A_{\perp}^{M}	$A_{\text{iso}}^{\text{M}}$
$^{187}\text{ReNF}_4^-$	PBE0	in vacuo	−324	−115	−185	−2792	−1355	−1834
		IEF-PCM ^b	−333	−112	−186	−2831	−1379	−1863
	PBE0-40HF	in vacuo	−349	−120	−196	−3099	−1643	−2128
		IEF-PCM ^b	−358	−118	−198	−3147	−1675	−2166
	Expt.^{c,e}	CH₃CN	−353	−132	−206	−3079	−1637	−2118
$^{187}\text{ReNCl}_4^-$	PBE0	in vacuo	−64	−70	−68	−2007	−872	−1250
		IEF-PCM ^b	−63	−69	−67	−2011	−871	−1251
	PBE0-40HF	in vacuo	−92	−76	−81	−2285	−1118	−1507
		IEF-PCM ^b	−92	−75	−81	−2290	−1119	−1510
	Expt.^{d,e}	CH₃CN	−93	−68	−77	−2308	−1145	−1533

^aThis work. All calculations were done at the 4c-DKS/Dyall(vTZ)/upcJ-2 level with or without the IEF-PCM solvation model, employing the traditional PBE0 hybrid functional or PBE0-40HF with a customised (40%) admixture of Hartree–Fock exchange.

^bThe value of the static permittivity $\epsilon_r = 37.5$ used for CH₃CN as solvent.

^cExperimental value taken from [124].

^dExperimental value taken from [125].

^eExperimental errors: $\Delta g_i \pm 3$ ppt, $A_i^{\text{M}} = \pm 15$ MHz; estimated from line-width analysis.

series. Our previous conclusion on the ‘best performing’ hybrid DFT functionals (with an optimal Hartree–Fock exchange admixture of about 25%–40% for g -tensors and 40% for HFCs) for selected d^1 compounds remains valid and virtually unaffected by the inclusion of direct solvent effects [24].

In contrast, we found a notable effect of the solvent polarity on electronic g -tensor components within a series of low-spin Ru and Os complexes (see Figure 1 for the structures). The results computed *in vacuo* and using the PCM solvent model for selected nitrosyl complexes, characterised experimentally by EPR spectroscopy in

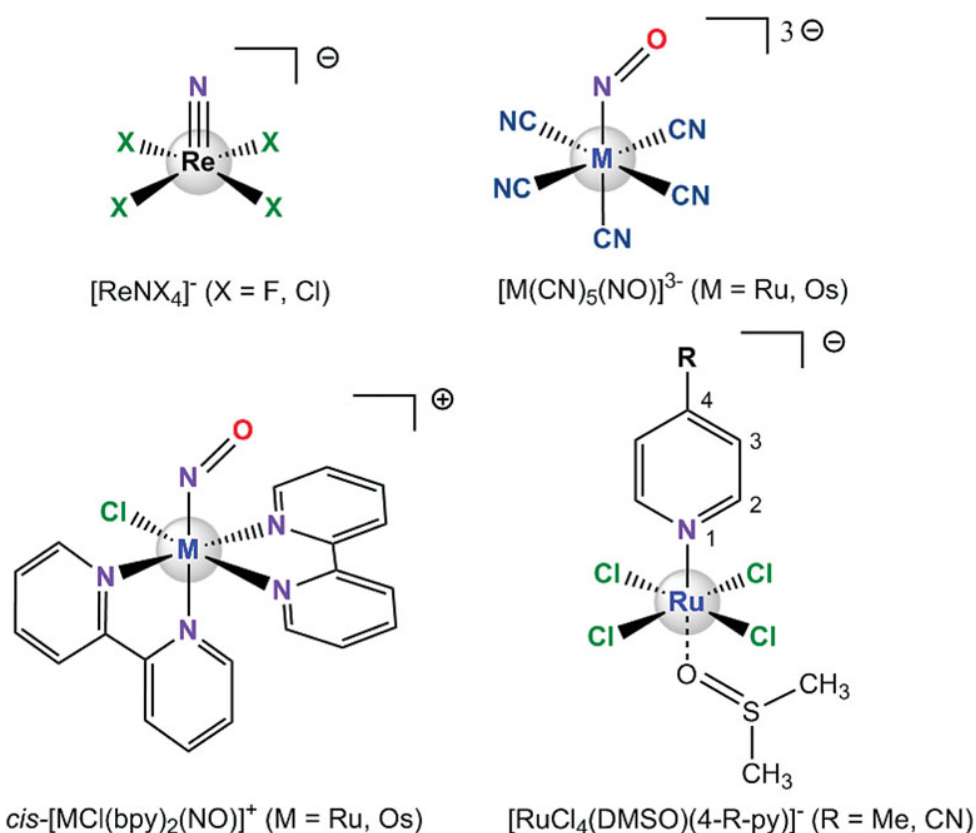
**Figure 1.** Schematic structures of the investigated transition metal complexes. Atom numbering in ligands of two Ru(III) complexes employed in pNMR calculations is given as well.

Table 2. Effect of a polarisable continuum solvent model (IEF-PCM) on computed principal components of the electronic Δg tensor (ppt) in selected Ru and Os nitrosyl complexes.^a

Complex	Method	Solvent	Δg_{11}	Δg_{22}	Δg_{33}	Δg_{iso}
$[\text{Ru}(\text{CN})_5(\text{NO})]^{3-}$	PBE0	in vacuo	−161	−22	−5	−63
		IEF-PCM ^b	−143	−16	−7	−55
	PBE0-40HF	in vacuo	−180	−27	−4	−70
		IEF-PCM ^b	−152	−17	−8	−59
	Expt.^c	CH₃CN	−132	0	2	−44
$[\text{Os}(\text{CN})_5(\text{NO})]^{3-}$	PBE0	in vacuo	−411	−87	−31	−177
		IEF-PCM ^b	−358	−69	−33	−153
	PBE0-40HF	in vacuo	−488	−98	−32	−206
		IEF-PCM ^b	−381	−74	−30	−162
	Expt.^c	CH₃CN	−368	−71	−43	−161
<i>cis</i> - $[\text{RuCl}(\text{bpy})_2(\text{NO})]^+$	PBE0	in vacuo	−113	−22	17	−39
		IEF-PCM ^b	−122	−24	17	−43
	PBE0-40HF	in vacuo	−131	−26	17	−47
		IEF-PCM ^b	−138	−29	18	−50
	Expt.^d	CH₃CN	−121	−10	27	−35
<i>cis</i> - $[\text{OsCl}(\text{bpy})_2(\text{NO})]^+$	PBE0	in vacuo	−268	−71	9	−110
		IEF-PCM ^b	−332	−90	8	−138
	PBE0-40HF	in vacuo	−332	−89	13	−136
		IEF-PCM ^b	−401	−113	22	−164
	Expt.^{e,f}	CH₃CN	−382	−112	−22	−172

^aThis work. All calculations were done at the 4c-DKS/Dyall(vTZ)/upcJ-2 level with or without the IEF-PCM solvation model, employing the traditional PBE0 hybrid functional or PBE0-40HF with a customised (40%) admixture of Hartree–Fock exchange.

^bThe value of the static permittivity $\epsilon_r = 37.5$ used for CH₃CN as solvent.

^cExperimental value taken from [126].

^dExperimental value taken from [117].

^eExperimental value taken from [127].

^fExperimental errors: $\Delta g_i \pm 10$ ppt; estimated from line-width analysis.

highly polar acetonitrile frozen solutions, are presented in Table 2. It is obvious that both relativistic and matrix effects are required to reproduce the experimental values in these systems. In general, solvent shifts of several tens of ppt are observed for the Δg_{11} component and amount up to 109 ppt in $[\text{Os}(\text{CN})_5(\text{NO})]^{3-}$ at the PBE0-40HF level. Such a solvent shift corresponds to a ca. 25% contribution to the overall g_{11} value and it is larger than the effect of Hartree–Fock exchange admixture or the variation of the Δg_{11} values in Ru nitrosyl complexes upon ligand substitution [117]. Note that the Δg_{11} axis lies in the M–N–O plane and it is nearly parallel to the N–O bond; (cf. Figure 2(a)). A smaller, but still remarkable, solvent effect is also noticed for Δg_{22} and Δg_{iso} values in Os complexes. Interestingly, the solvent effect on Δg_{11} and Δg_{22} in anionic $[\text{M}(\text{CN})_5(\text{NO})]^{3-}$ species have positive values, while they are negative in cationic $[\text{MCl}(\text{bpy})_2(\text{NO})]^+$ complexes. Nevertheless, the use of the PCM improves the agreement of computed g -tensor shifts with experimental data in both cases and demonstrates the sensitivity of EPR parameters to solvent polarity in these systems (see Table 2 and Figure 2).

We note in passing, that sizeable solvent effects on the electronic g -tensor and metal HFCs were found, e.g. for some Cu(II) complexes, but these were primarily caused by the change of the metal coordination environment

(upon solvent coordination or protonation of ligands) rather than by solvent polarity alone, as also confirmed by DFT calculations. Here, the PCM is not sufficient to reproduce the observed trends and explicit solvent molecules have to be considered in the calculations [118–120].

Due to the lack of experimental data on HFCs in the investigated nitrosyl complexes, benchmark studies were also performed for the temperature-dependent part of pNMR shifts, which are for doublets inherently associated with the product of the electronic g -tensor and HFC tensor of the nucleus in question (see Equation (29)). As model systems, we selected two Ru(III) low-spin d^5 complexes ($S = 1/2$) studied comprehensively for their ^1H and ^{13}C NMR shifts in highly polar dimethylformamide (DMF) as a function of temperature [67]. Experimental temperature-dependent pNMR shifts along with computed data *in vacuo* and in solution are collected in Table 3. A significant improvement of the computed pNMR shifts upon inclusion of bulk solvent effects can be noticed; the mean absolute error (MAE) is reduced from 10–20 ppm to about 2–4 ppm. These MAEs are comparable to or slightly better than errors obtained by using the COSMO solvation model in conjunction with the two-component ZORA-SO Hamiltonian, implemented in the ADF software package. Closer inspection (see Tables 1

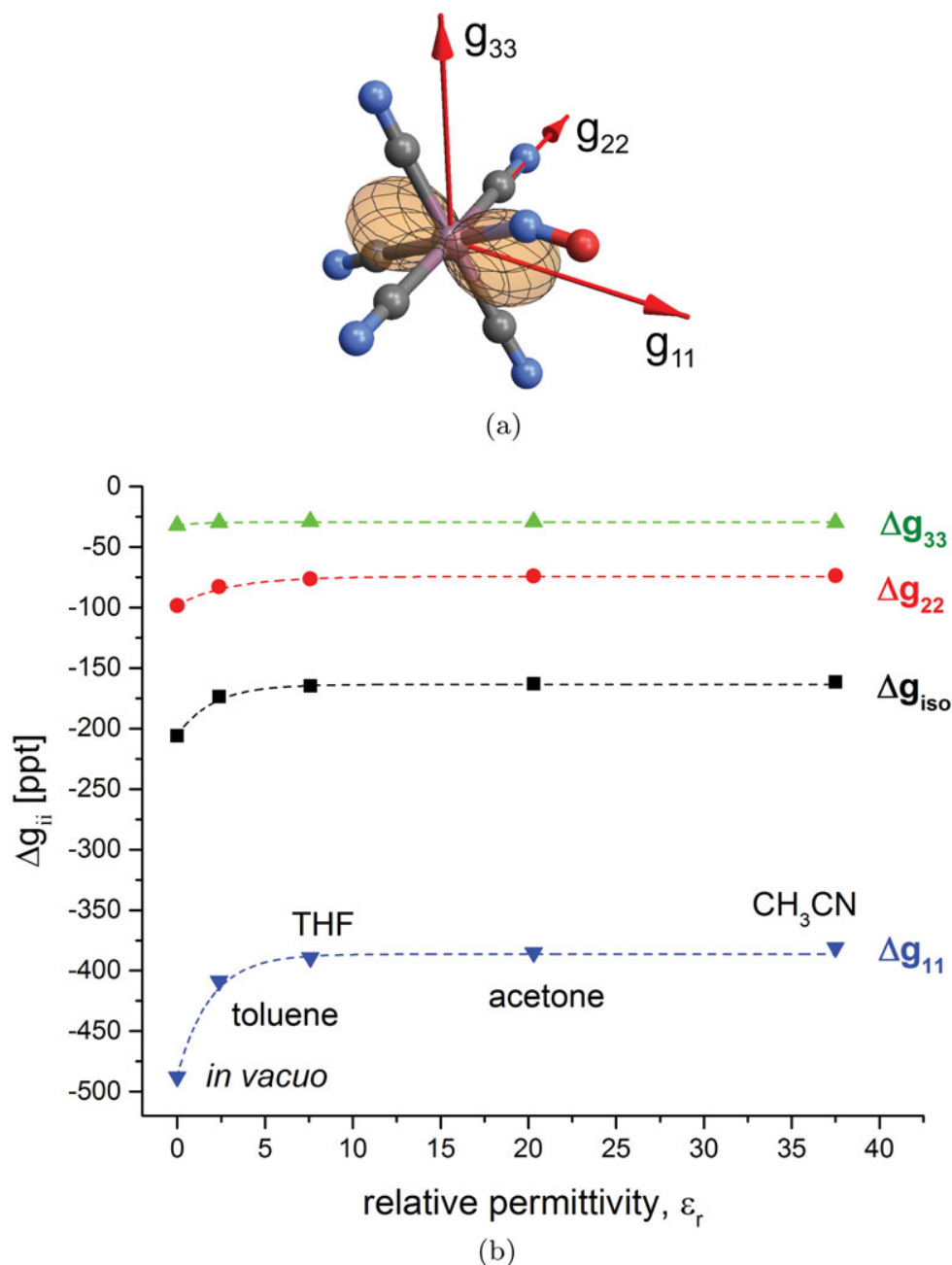


Figure 2. (a) Visualisation of the electronic Δg -tensor and its principal axes in $[\text{Os}(\text{CN})_5(\text{CN})]^{3-}$. (b) The dependency of Δg_{ii} values on solvent polarity.

and 2 in Supporting Information) revealed that these solvent shifts are governed by changes in both the electronic g -tensor and HFC tensors of the ligand atoms, the latter being more dominant. HFCs are affected more by solvent polarity than the g -tensor components in relative terms; e.g. the solvent shifts are about 5% for g_{iso} , whereas they contribute more than 50% to A_{iso} in some cases. Interestingly, apart from changing the magnitude of the pNMR shifts, bulk solvent effects may also invert their sign due

to a change of the spin density distribution in response to the solvent polarity, as demonstrated, for example, for C3 in the 4-CN-substituted pyridine complex.

Finally, we note that the choice of atomic van der Waals radii used in the construction of the molecular-solvent-accessible surface can have a substantial impact on the calculated results. In the systems studied, using the universal force field (UFF)-derived radii [121] provides results that do not compare as well to

Table 3. Effect of various solvent models on computed ^1H and ^{13}C temperature-dependent contribution to pNMR shifts (ppm) in selected Ru(III) complexes.^a

Complex	Nucleus	Solvation model				Expt. ^e
		<i>In vacuo</i> ^a	IEF-PCM ^{a, b}	IEF-PCM ^{a, c}	COSMO ^d	
[RuCl ₄ (DMSO)(4-Me-py)] [−]	H2	−6.7	−11.6	−14.1	−14.8	−14.0
	H3	−8.9	−9.5	−10.3	−9.7	−9.4
	H _{Me}	−8.5	−6.6	−6.2	−6.1	−6.0
	H _{DMSO}	−12.4	−14.3	−15.6	−17.1	−15.5
	C2	−73	−70	−74	−75	−72
	C3	−7	−19	−23	−28	−25
	C4	−49	−33	−30	−28	−27
	C _{Me}	11	4	1	2	0
	C _{DMSO}	−180	−162	−150	−163	−156
	MAE^f	9.9	3.2	1.8	2.1	
[RuCl ₄ (DMSO)(4-CN-py)] [−]	H2	−1.8	−7.3	−10.8	−10.8	−11.9
	H3	−9.7	−9.8	−10.3	−9.9	−8.5
	H _{DMSO}	−12.4	−14.2	−15.5	−16.9	−15.7
	C2	−84	−81	−84	−86	−78
	C3	13	−4	−12	−15	−17
	C4	−78	−52	−42	−42	−34
	C _{CN}	52	29	20	21	11
	C _{DMSO}	−175	−159	−148	−160	−146
	MAE^f	20.6	9.0	3.8	5.7	

^aThis work. Data calculated at the 4c-DKS/Dyall(vTZ)/upcJ-2 level of theory with the PBE0 hybrid functional.^bIEF-PCM using a solvent-accessible surface with UFF radii [121]: 1.4430 Å for H, 1.4815 Å for Ru, 1.9255 Å for C, 2.0175 Å for S, 1.75 Å for O, 1.9735 Å for Cl and 1.83 Å for N. All radii were multiplied by a factor of 1.2. The value of the static permittivity for DMF ($\epsilon_r = 37.0$) was used.^cIEF-PCM using a solvent-accessible surface with radii from Allinger's MM3 model [116] (see Section 3 for more details). The value of the static permittivity for DMF ($\epsilon_r = 37.0$) was used.^dCalculations at the ZORA-SO/PBE0/TZ2P level of theory with the COSMO solvation model. [67] A Delley surface [128] with radii from Allinger's MM3 model was used [116] (see Section 3 for more details). The value of the static permittivity for DMF ($\epsilon_r = 37.0$) was used.^eExperimental data measured in dimethylformamide and taken from [67]^fMean absolute error between calculated and experimental data.

experiments as when using the radii derived from Allinger's MM3 model [116].

5. Summary

We have presented an extension of the polarisable continuum model for solvation to the calculation of EPR *g*-tensors and HFC constants as well as the temperature-dependent contribution to paramagnetic NMR chemical shifts at the relativistic four-component DFT level. The small-component basis set is generated at the integral level by imposing the restricted kinetic balance condition, allowing for efficient calculations also for large molecular complexes. We have included the solvent effects by integrating the four-component relativistic DFT program ReSpect [77] with the stand-alone library PCM-Solver [78]. The formalism is general and although results have been presented only for the IEF-PCM model, the implementation is also applicable for the COSMO model.

Our results show that the importance of direct solvent effects to EPR parameters and pNMR shifts as described by the PCM is difficult to predict *a priori*, even though

they are in many cases significant, amounting up to 25% of the gas-phase value, as demonstrated for the selected Ru and Os complexes. In other cases, such as the [MEX_n]^q d¹ complexes, there is hardly any noticeable direct solvent effect. The results presented in this contribution demonstrate the need to explore the relevance of solvent effects when computing EPR and pNMR parameters. The PCM provides a cost-effective strategy to carry out such an analysis and to possibly rule out whether consideration of solvent effects is mandatory or not. For pNMR chemical shifts, we found solvent effects to be sizeable, mandating their inclusion in precise calculations and/or reliable predictions and analysis. In addition, we observed an important role of van der Waals atomic radii employed in the construction of solvent-accessible surfaces, where results obtained by means of the UFF radii are notably outperformed by those using the radii derived from Allinger's MM3 model.

A detailed comparison with experiment is still difficult. One reason for this is our restriction to direct solvation effects. However, many experimental EPR studies are conducted in solid matrices of the solute embedded in the solvent. It is not clear whether PCM would in this

case be able to accurately model such medium effects. We also note that for charged metal complexes, the solvent molecules may directly coordinate with the complex, giving rise to changes in the molecular properties that arise from strong interactions with the electron density of the solute, which cannot be described by a dielectric continuum model alone. In this case, supermolecular complexes embedded in a dielectric continuum may be a good model to account for such effects.

In view of the fact that zero-point vibrational corrections have been shown to be important for HFC constants [122,123], it can be expected that also geometry relaxation due to solvation can be significant to the EPR and temperature-dependent pNMR studies. The extension of the PCM model to geometry optimisations at the four-component level of theory is in progress in our group.

Acknowledgment

We would like to dedicate this work to our good friend and colleague, Dr. Hans Jørgen Aagaard Jensen, on the occasion of his 60th birthday.

Disclosure statement

No potential conflict of interest was reported by the authors.

Funding

This work was supported by the Research Council of Norway (RCN) through a Center of Excellence (CoE) Grant and project grants [grant number 179568], [grant number 214095]. The computational resources for this project have been provided by the NOTUR high-performance computing program [grant number NN4654K]. L. F. also acknowledges financial support by the Tromsø Research Foundation (SURFINT grant). P. H. acknowledges support from the Berlin DFG excellence cluster on Unifying Concepts in Catalysis (UniCat) and DFG project KA1187/13-1.

References

- [1] J.E. Harriman, *Theoretical Foundations of Electron Spin Resonance* (Academic Press, New York, 1978).
- [2] F.E. Mabbs and D. Collison, in *Studies in Inorganic Chemistry*, Vol. 16 (Elsevier, Amsterdam, 1992).
- [3] M. Kaupp, M. Bühl and V. G. Malkin, editors, *Calculation of NMR and EPR Parameters* (Wiley-VCH Verlag GmbH & Co. KGaA, Weinheim, 2004).
- [4] G. Hanson and L. Berliner, *Metals in Biology: Applications of High Resolution EPR to metalloenzymes*, Vol. 29 (Springer, New York, 2010).
- [5] F. Neese, J.M. Zaleski, K.L. Zaleski and E.I. Solomon, *J. Am. Chem. Soc.* **122**, 11703 (2000).
- [6] G. Schreckenbach and T. Ziegler, *J. Phys. Chem. A* **101**, 3388 (1997).
- [7] O.L. Malkina, J. Vaara, B. Schimmelpfennig, M. Munzarova, V.G. Malkin and M. Kaupp, *J. Am. Chem. Soc.* **122**, 9206 (2000).
- [8] F. Neese, *J. Chem. Phys.* **115**, 11080 (2001).
- [9] S. Patchkovskii and T. Ziegler, *J. Phys. Chem. A* **105**, 5490–5497 (2001).
- [10] F. Neese, *J. Chem. Phys.* **118**, 3939 (2003).
- [11] A.V. Arbuznikov, J. Vaara and M. Kaupp, *J. Chem. Phys.* **120**, 2127–2139 (2004).
- [12] Z. Rinkevicius, L. Telyatnyk, O. Vahtras and H. Ågren, *J. Chem. Phys.* **121**, 7614–7623 (2004).
- [13] Z. Rinkevicius, K.J. de Almeida and O. Vahtras, *J. Chem. Phys.* **129**, 064109 (2008).
- [14] Z. Rinkevicius, K. J. de Almeida, C.I. Oprea, O. Vahtras, H. Ågren and K. Ruud, *J. Chem. Theory Comput.* **4**, 1810–1828 (2008).
- [15] L.F. Chibotaru and L. Ungur, *J. Chem. Phys.* **137**, 064112 (2012).
- [16] H. Bolvin, *ChemPhysChem* **7**, 1575–1589 (2006).
- [17] S. Vancoillie, P.-Å. Malmqvist and K. Pierloot, *ChemPhysChem* **8**, 1803–1815 (2007).
- [18] F. Gendron, B. Pritchard, H. Bolvin and J. Autschbach, *Inorg. Chem.* **53**, 8577–8592 (2014).
- [19] K. Sharkas, B. Pritchard and J. Autschbach, *J. Chem. Theory Comput.* **11**, 538–549 (2015).
- [20] T. Yanai, Y. Kurashige, W. Mizukami, J. Chalupský, T.N. Lan and M. Saitow, *Int. J. Quantum Chem.* **115**, 283–299 (2015).
- [21] T.N. Lan, Y. Kurashige and T. Yanai, *J. Chem. Theory Comput.* **10**, 1953–1967 (2014).
- [22] S. Patchkovskii and T. Ziegler, *J. Chem. Phys.* **111**, 5730 (1999).
- [23] P. Hrobarik, M. Repisky, S. Komorovsky, V. Hrobarikova and M. Kaupp, *Theor. Chem. Acc.* **129**, 715–725 (2011).
- [24] S. Gohr, P. Hrobarik, M. Repisky, S. Komorovsky, K. Ruud and M. Kaupp, *J. Phys. Chem. A* **119**, 12892–12905 (2015).
- [25] E. Van Lenthe, P.E. Wormer and A. Van Der Avoird, *J. Chem. Phys.* **107**, 2488–2498 (1997).
- [26] E. van Lenthe, A. Van Der Avoird and P.E. Wormer, *J. Chem. Phys.* **108**, 4783–4796 (1998).
- [27] K.M. Neyman, D.I. Ganyushin, A.V. Matveev and V.A. Nasluzov, *J. Phys. Chem. A* **106**, 5022–5030 (2002).
- [28] I. Malkin, O.L. Malkina, V.G. Malkin and M. Kaupp, *Chem. Phys. Lett.* **396**, 268–276 (2004).
- [29] I. Malkin, O.L. Malkina, V.G. Malkin and M. Kaupp, *J. Chem. Phys.* **123**, 244103 (2005).
- [30] B. Sandhoefer and F. Neese, *J. Chem. Phys.* **137**, 094102 (2012).
- [31] P. Verma and J. Autschbach, *J. Chem. Theory Comput.* **9**, 1932–1948 (2013).
- [32] P. Verma and J. Autschbach, *J. Chem. Theory Comput.* **9**, 1052–1067 (2013).
- [33] R. Arratia-Perez and D.A. Case, *J. Chem. Phys.* **79**, 4939–4949 (1983).
- [34] H. Quiney, *Chem. Phys. Lett.* **353**, 253–258 (2002).
- [35] M. Repisky, S. Komorovsky, E. Malkin, O.L. Malkina and V.G. Malkin, *Chem. Phys. Lett.* **488**, 94–97 (2010).
- [36] E. Malkin, M. Repisky, S. Komorovsky, P. Mach, O.L. Malkina and V.G. Malkin, *J. Chem. Phys.* **134**, 044111 (2011).

- [37] M.S. Vad, M.N. Pedersen, A. Nørager, and H.J.A. Jensen, *J. Chem. Phys.* **138**, 214106 (2013).
- [38] S. Moon and S. Patchkovskii, in *Calculation of NMR and EPR Parameters. Theory and Applications*, edited by M. Kaupp, M. Bühl and V.G. Malkin (Wiley-VCH, Weinheim, 2004), Chapter 20.
- [39] W. Van Den Heuvel and A. Soncini, *Phys. Rev. Lett.* **109**, 073001 (2012).
- [40] W. Van Den Heuvel and A. Soncini, *J. Chem. Phys.* **138**, 054113 (2013).
- [41] F. Gendron, K. Sharkas and J. Autschbach, *J. Phys. Chem. Lett.* **6**, 2183–2188 (2015).
- [42] T.O. Pennanen and J. Vaara, *J. Chem. Phys.* **123**, 174102 (2005).
- [43] P. Hrobarik, R. Reviakine, A.V. Arbuznikov, O.L. Malkina, V.G. Malkin, F.H. Köhler and M. Kaupp, *J. Chem. Phys.*, **126**, 024107 (2007).
- [44] J. Autschbach, S. Patchkovskii and B. Pritchard, *J. Chem. Theory Comput.* **7**, 2175–2188 (2011).
- [45] S. Komorovsky, M. Repisky, K. Ruud, O.L. Malkina and V.G. Malkin, *J. Phys. Chem. A* **117**, 14209 (2013).
- [46] J. Vaara, S.A. Rouf, and J. Mareš, *J. Chem. Theory Comput.* **11**, 4840–4849 (2015).
- [47] S.A. Rouf, J. Mareš and J. Vaara, *J. Chem. Theory Comput.* **11**, 1683–1691 (2015).
- [48] C. Reichardt and T. Welton, *Solvents and Solvent Effects in Organic Chemistry* Wiley-VCH Verlag GmbH & Co. KGaA, Weinheim, 2004, pp. 191–208, 2010).
- [49] B. Mennucci, J. Martínez and J. Tomasi, *J. Phys. Chem. A* **105**, 7287–7296 (2001).
- [50] I. Ciofini, in *Calculation of NMR and EPR Parameters. Theory and Applications*, (Wiley-VCH Verlag GmbH & Co. KGaA, Weinheim, 2004), pp. 191–208.
- [51] J. Sadlej and M. Pecul, in *Computational Modelling of the Solvent–Solute Effect on NMR Molecular Parameters by a Polarizable Continuum Model*, edited by B. Mennucci and R. Cammi, (John Wiley & Sons, Ltd, 2007), pp. 125–145.
- [52] V. Barone, P. Cimino, and M. Pavone, in *Continuum Solvation Models in Chemical Physics*, edited by B. Mennucci and R. Cammi (John Wiley & Sons, Ltd, Chichester, 2007), p. 145.
- [53] E. Pauwels, T. Verstraelen, H. De Cooman, V. Van Speybroeck, and M. Waroquier, *J. Phys. Chem. B* **112**, 7618–7630 (2008).
- [54] H.M. Senn and W. Thiel, *Angew. Chem. Int. Edit.* **48**, 1198–1229 (2009).
- [55] J. Tomasi, B. Mennucci and R. Cammi, *Chem. Rev.* **105**, 2999–3094 (2005).
- [56] S. Sinnecker and F. Neese, *J. Comput. Chem.* **27**, 1463–1475 (2006).
- [57] C. Houriez, N. Ferré, M. Masella and D. Siri, *J. Chem. Phys.* **128**, 244504 (2008).
- [58] E. Pauwels, R. Declerck, T. Verstraelen, B. De Sterck, C.W. Kay, V. Van Speybroeck and M. Waroquier, *J. Phys. Chem. B* **114**, 16655–16665 (2010).
- [59] Z. Rinkevicius, N.A. Murugan, J. Kongsted, K. Aidas, A.H. Steindal, and H. Ågren, *J. Phys. Chem. B*, **115**, 4350–4358 (2011).
- [60] Z. Rinkevicius, N.A. Murugan, J. Kongsted, B. Frecus, A.H. Steindal and H. Ågren, *J. Chem. Theory Comput.* **7**, 3261–3271 (2011).
- [61] F. Lipparini, C. Cappelli and V. Barone, *J. Chem. Phys.* **138**, 234108 (2013).
- [62] B. Mennucci R. Cammi, editors, *Continuum Solvation Models in Chemical Physics*, (John Wiley & Sons, Ltd, Chichester, 2007).
- [63] C. Amovilli and B. Mennucci, *J. Phys. Chem. B* **101**, 1051–1057 (1997).
- [64] V. Weijs, B. Mennucci and L. Frediani, *J. Chem. Theory Comput.* **6**, 3358–3364 (2010).
- [65] C. Adamo, M. Heitzmann, F. Meilleur, N. Rega, G. Scalmani, A. Grand, J. Cadet and V. Barone, *J. Am. Chem. Soc.* **123**, 7113–7117 (2001).
- [66] M. Kaupp, C. Remenyi, J. Vaara, O.L. Malkina and V.G. Malkin, *J. Am. Chem. Soc.* **124**, 2709–2722 (2002).
- [67] J. Novotny, M. Sojka, S. Komorovsky, M. Necas and R. Marek, *J. Am. Chem. Soc.* **138**, 8432–8445 (2016).
- [68] J. Autschbach and T. Ziegler, *J. Am. Chem. Soc.* **123**, 3341–3349 (2001).
- [69] J. Autschbach and B. Le Guennic, *J. Am. Chem. Soc.* **125**, 13585–13593 (2003).
- [70] A. Antušek, M. Pecul and J. Sadlej, *Chem. Phys. Lett.* **427**, 281–288 (2006).
- [71] J. Autschbach and M. Sterzel, *J. Am. Chem. Soc.* **129**, 11093–11099 (2007).
- [72] M. Olejniczak and M. Pecul, *Chemphyschem* **10**, 1247–1259 (2009).
- [73] S. Zheng and J. Autschbach, *Chem. Eur. J.* **17**, 161–173 (2011).
- [74] J. Vicha, M. Patzschke and R. Marek, *Phys. Chem. Chem. Phys.* **15**, 7740–7754 (2013).
- [75] J. Vicha, J. Novotny, M. Straka, M. Repisky, K. Ruud, S. Komorovsky and R. Marek, *Phys. Chem. Chem. Phys.* **17**, 24944–24955 (2015).
- [76] R. Di Remigio, R. Bast, L. Frediani and T. Saue, *J. Phys. Chem. A* **119**, 5061–5077 (2015).
- [77] ReSpect, version 3.5.0 (2016) – Relativistic Spectroscopy DFT program of authors Repisky, M.; Komorovsky, S.; Malkin, V. G.; Malkina, O. L.; Kaupp, M.; Ruud, K., with contributions from Bast, R.; Ekström, U.; Kadek, M.; Knecht, S.; Konecny, L.; Malkin, E.; Malkin-Ondik, I.; Remigio, R. Di. <http://www.respectprogram.org>.
- [78] PCMSolver, an Application Programming Interface for the Polarizable Continuum Model electrostatic problem, written by R. Di Remigio, L. Frediani and K. Mozgawa. <http://pcmsolver.readthedocs.org/>
- [79] J. Tomasi and M. Persico, *Chem. Rev.* **94**, 2027–2094 (1994).
- [80] J.D. Jackson, *Classical Electrodynamics* (John Wiley & Sons, New York, 1998).
- [81] J. Vanderlinde, *Classical Electromagnetic Theory* (Springer, Dordrecht, 2005).
- [82] E. Cancès and B. Mennucci, *J. Math. Chem.* **23**, 309 (1998).
- [83] W. Hackbusch, *Integral Equations – Theory and Numerical Treatment* (Birkhäuser, Basel, 1995).
- [84] G.C. Hsiao and W.L. Wendland, *Boundary Integral Equations*, Vol. 164 (Springer, Berlin, 2008).
- [85] L. Frediani, R. Cammi, S. Corni and J. Tomasi, *J. Chem. Phys.* **120**, 3893–3907 (2004).
- [86] R. Di Remigio, K. Mozgawa, H. Cao, V. Weijs and L. Frediani, 2016, (submitted).

- [87] A. Delgado, S. Corni and G. Goldoni, *J. Chem. Phys.* **139**, 024105 (2013).
- [88] A. Ern and J.-L. Guermond, *Theory and Practice of Finite Elements* (Springer, New York, 2004).
- [89] E. Silla, J.L. Pascual-Ahuir, J. Tomasi and R. Bonaccorsi, *J. Comp. Chem.* **8**, 778–787 (1987).
- [90] C.S. Pomelli, in *Continuum Solvation Models in Chemical Physics*, edited by B. Mennucci and R. Cammi (John Wiley & Sons, Ltd, Chichester, 2007), pp. 49–63.
- [91] A. Klamt and G. Schüürmann, *J. Chem. Soc. Perkin Trans. 2*, 799–805 (1993).
- [92] C.C. Pye and T. Ziegler, *Theor. Chem. Acc.* **101**, 396–408 (1999).
- [93] M. Cossi, N. Rega, G. Scalmani and V. Barone, *J. Comput. Chem.* **24**, 669–81 (2003).
- [94] T. Helgaker, P. Jørgensen and J. Olsen, *Molecular Electronic-Structure Theory* (John Wiley & Sons, Ltd, Chichester, 2000).
- [95] K.G. Dyall and K. Fægri, Jr, *An Introduction to Relativistic Quantum Chemistry* (Oxford University Press, New York, 2007).
- [96] M. Reiher and A. Wolf, *Relativistic Quantum Chemistry* (Wiley-VCH Verlag GmbH & Co. KGaA, Weinheim, 2009).
- [97] P. Cherry, S. Komorovsky, V.G. Malkin and O.L. Malkina, *Mol. Phys.* **2016**, doi:10.1080/00268976.2016.1191688
- [98] V.A. Dzuba, V.V. Flambaum and O.P. Sushkov, *J. Phys. B* **17**, 1953–1968 (1984).
- [99] L.M. Sandratskii, *Adv. Phys.* **47**, 91–160 (1998).
- [100] C. van Wüllen, *J. Comput. Chem.* **23**, 779–785 (2002).
- [101] G. Scalmani and M.J. Frisch, *J. Chem. Theory Comput.* **8**, 2193–2196 (2012).
- [102] H.M. McConnell and D.B. Chesnut, *J. Chem. Phys.* **28**, 107–117 (1958).
- [103] H.M. McConnell and R.E. Robertson, *J. Chem. Phys.* **29**, 1361–1365 (1958).
- [104] R.J. Kurland and B.R. McGarvey, *J. Magn. Reson.* **2**, 286–301 (1970).
- [105] J.P. Perdew, K. Burke and M. Ernzerhof, *Phys. Rev. Lett.* **77**, 3865–3868 (1996).
- [106] C. Adamo and V. Barone, *J. Chem. Phys.* **110**, 6158–6169 (1999).
- [107] S. Grimme, J. Antony, S. Ehrlich, and H. Krieg, *J. Chem. Phys.* **132**, 154104 (2010).
- [108] S. Grimme, S. Ehrlich, and L. Goerigk, *J. Comput. Chem.* **32**, 1456–1465 (2011).
- [109] D. Andrae, U. Häußermann, M. Dolg, H. Stoll and H. Preuß, *Theor. Chim. Acta* **77**, 123–141 (1990).
- [110] F. Weigend and R. Ahlrichs, *Phys. Chem. Chem. Phys.* **7**, 3297–3305 (2005).
- [111] L. Visscher and K. G. Dyall, *At. Data Nucl. Data Tables* **67**, 207–224 (1997).
- [112] F. Jensen, *J. Chem. Theory Comput.* **1360–1369** (2006).
- [113] K.G. Dyall, *Theor. Chem. Acc.* **117**, 483–489 (2006).
- [114] K.G. Dyall, *Theor. Chem. Acc.* **112**, 403–409 (2004).
- [115] K.G. Dyall and A. S. P. Gomes, *Theor. Chem. Acc.* **125**, 97–100 (2010).
- [116] N.L. Allinger, X. Zhou and J. Bergsma, *J. Mol. Struct.: THEOCHEM* **312**, 69–83 (1994).
- [117] S. Frantz, B. Sarkar, M. Sieger, W. Kaim, F. Roncaroli, J.A. Olabe and S. Zális, *Eur. J. Inorg. Chem.* **2004**, 2902–2907 (2004).
- [118] W.M. Ames and S.C. Larsen, *J. Phys. Chem. A* **113**, 4305–4312 (2009).
- [119] K.J. de Almeida, T.C. Ramalho, Z. Rinkevicius, O. Vahtras, H. Ågren and A. Cesar, *J. Phys. Chem. A* **115**, 1331–1339 (2011).
- [120] C. Finazzo, C. Calle, S. Stoll, S. Van Doorslaer and A. Schweiger, *Phys. Chem. Chem. Phys.* **8**, 1942–1953 (2006).
- [121] A.K. Rappe, C.J. Casewit, K.S. Colwell, W.A. Goddard and W.M. Skiff, *J. Am. Chem. Soc.* **114**, 10024–10035 (1992).
- [122] X. Chen, Z. Rinkevicius, Z. Cao, K. Ruud and H. Ågren, *Phys. Chem. Chem. Phys.* **13**, 696–707 (2010).
- [123] X. Chen, Z. Rinkevicius, K. Ruud, and H. Ågren, *J. Chem. Phys.* **138**, 054310 (2013).
- [124] A. Voigt, U. Abram, and R. Kirmse, *Inorg. Chem. Commun.* **1**, 141–142 (1998).
- [125] G.M. Lack and J.F. Gibson, *J. Mol. Struct.* **46**, 299–306 (1978).
- [126] M. Wanner, T. Scheiring, W. Kaim, L.D. Slep, L.M. Baraldo, J.A. Olabe, S. Zális and E.J. Baerends, *Inorg. Chem.* **40**, 5704–5707 (2001).
- [127] P. Singh, B. Sarkar, M. Sieger, M. Niemeyer, J. Fiedler, S. Zális and W. Kaim, *Inorg. Chem.* **45**, 4602–4609 (2006).
- [128] B. Delley, *Mol. Simul.* **32**, 117–123 (2006).